THE MARTIAN AIRGLOW AND SCATTERED SUNLIGHT : FUTURE OBSERVATIONS FROM A SPINNING ORBITER.

J.-Cl. Gérard

Institut d'Astrophysique - Université de Liège, Belgium.

ABSTRACT

The characteristics of the martian airglow on the day and night sides of the planet are reviewed on the basis of the observations made by previous missions and current atmospheric models.
The detectability of nitric oxide from its fluorescence spectrum is discussed is some details.
The aeronomical and meteorological importance of measuring the distribution of a few dayglow emissions is described. It is shown that limb scanning and backscattered ultraviolet methods may be used to derive the ozone and dust distribution in the lower atmosphere. A list of scientific objectives for a UV spectrometer on a low cost spinning Mars orbiter is given.

Keywords : Mars atmosphere, airglow, ozone, ultraviolet, spectrometer.

1. INTRODUCTION

The atmospheric ultraviolet and visible spectrum of the martian atmosphere has been observed by a series of American and Soviet space instruments. The two fly-by missions MARINER 6 and 7 provided in July and August 1969 the first spectra of the Mars upper atmosphere airglow below 3000 A. (Barth et al., 1971). The main features were identified as atomic lines of HI, OI, CI and molecular bands due to $CO(A^1\Pi)$, $CO(a^3\Pi)$, $CO^+(B^2\Sigma)$, CO_2^+ $(B^2\Sigma)$ and CO_2^+ $(A^2\Pi)$. From November 1971 until October 1972, the MARINER 9 spacecraft in orbit around the planet made extensive observations of the ultraviolet airglow and scattered sunlight. No new features were identified in the dayglow spectrum but their variability and the correlation between individual emission rates and solar activity was investigated (Barth et al., 1972; Stewart et al., 1972). The main conclusions were that, with the exception of OI 1304A and HI Lyα, all the emissions could be explained by the direct or indirect effect of solar ultraviolet radiation on carbon dioxide. The spectrum also indicated that CO_2 was the dominant constituent and that the Mars atmosphere is essentially undissociated. The hydrogen and atomic oxygen lines were attributed the resonance scattering of H and O produced by photodissociation of water vapor and carbon dioxide. A search for optical signatures of molecular nitrogen gave negative results, implying an N_2 mixing ratio between 0.5 and 5%, depending on the strength of the eddy mixing.
Another outstanding discovery of the MARINER 7 mission was the detection of ozone in the Mars lower atmosphere and the study of its latitudinal distribution from the MARINER 9 orbiter. It was found that the amount of ozone varied from less than 3µm-atm (the MARINER 9 detection limit) to about 60µm-atm (Barth et al. 1973).Comparison with the water vapor measurements made with the infrared spectrometer indicated that ozone is present when the atmosphere is dry and cold and decreases substantially when the amount of H_2O increases.
Extensive analysis of the solar scattered radiation were made during the 1971 Mars dust storm by matching the scattering albedo and phase function with Mie scattering calculations. The results indicated that the effective radius of the particles is about 1µm and the refraction index ≃1.8 and these aerosols have an aborption band in the ultraviolet.
The topography of the Mars surface was established with the MARINER 9 ultraviolet spectrometer by measuring the Rayleigh scattered signal at 3050 A during periods when the lower atmosphere was relatively free of dust. Under these conditions, the ultraviolet radiation is directly proportional to the atmospheric surface.
The Soviet MARS 3 orbiter carrying atomic hydrogen and oxygen resonance ultraviolet photometers made observations between December 1971 and March 1972. A visible spectrometer on board the MARS 5 orbiter did not detect any night airglow from the martian atmosphere and allowed upper limits to be set on the emission rates of the $O(^1S)$ and O_2 herzberg recombination airglow. A two-channel filter photometer was also included in the MARS 5 payload and provided two measurements of the ozone and aerosol vertical distributions. The observations indicated the presence of an ozone layer peaking near 38km exhibiting large O_3 densities compared to most theoretical model calculations.
The VIKING mission did not include any ultraviolet or visible spectrometer but new information on atmospheric composition was gathered by the neutral mass spectrometer and gas chromatograph. These new results stimulated reaximination of some of the observations collected previously and better definition of future needs for ultraviolet spectropho-

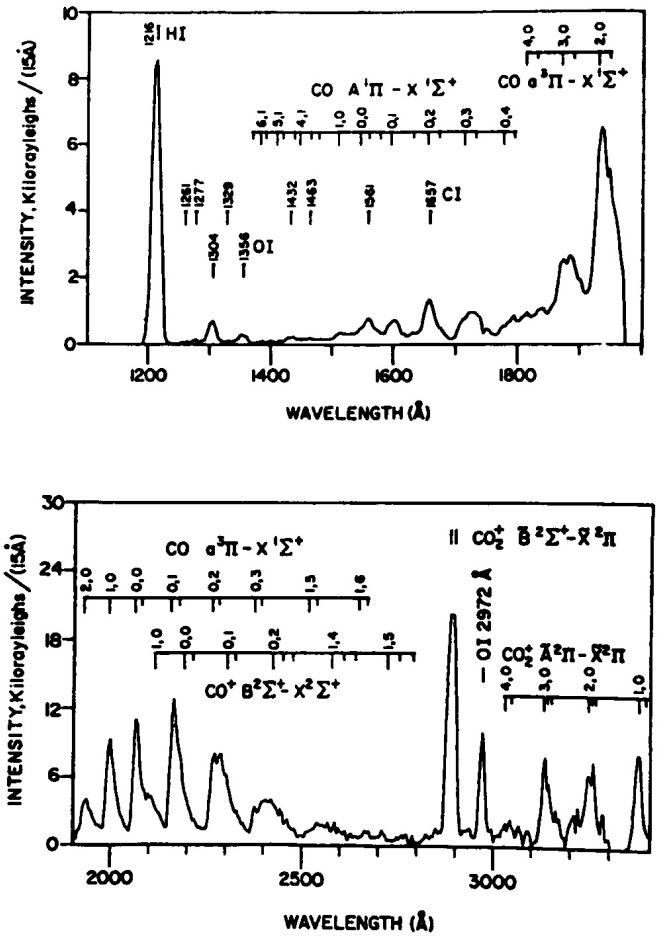

figure 1. : martian limb airglow spectrum observed with the MARINER 9 ultraviolet spectrometer.

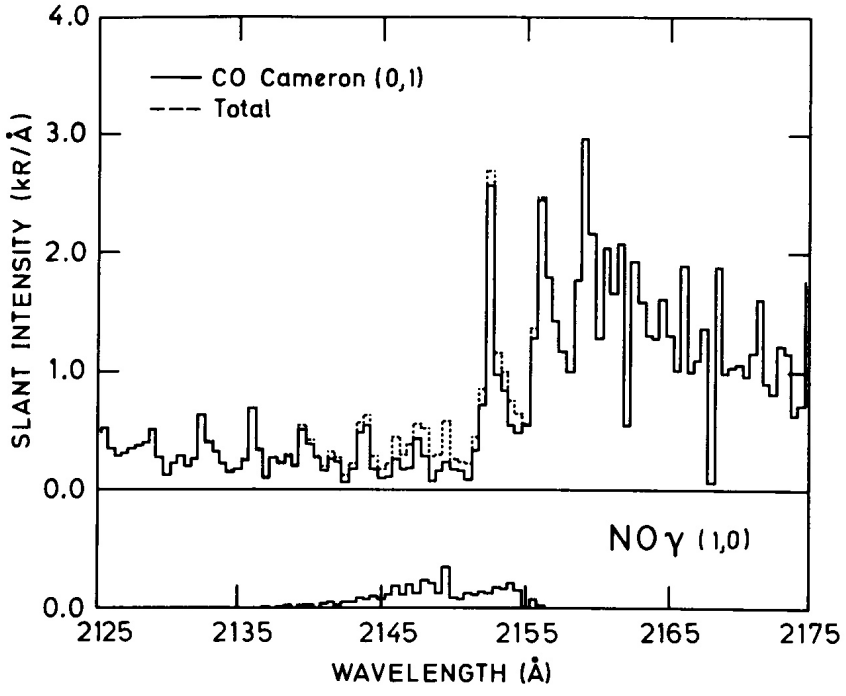

figure 2. : synthetic spectrum spectrum of the CO Cameron (0,1) band (solid line), NOγ (1,0) band and sum of the two contributions (dotted line) for a 0.5 Å resolution.

tometry. In the next sections, we review current knowledge and understanding of the martian airglow and atmospheric light scattering, insisting particularly on new developments and needs for future observations. Finally, it is shown that the constains to carry out the necessary measurements can be met with an versatile ultraviolet spectrophotometer on board a low cost spinning Mars orbiter.

2. THE MARS UPPER ATMOSPHERE AIRGLOW

2.1. The dayglow

As mentioned before, most of our knowledge of martian upper atmosphere airglow comes from the MARINER missions. Figure 1 shows a sum of 120 limb spectra obtained with the MARINER 9 UVS (Barth et al., 1972) at a 15-Å resolution. The excitation mechanisms for the CO, CO^+ and CO_2^+ are mainly (Stewart, 1972; Fox and Dalgarno, 1979)

$$CO_2 + h\nu(e) \rightarrow (CO_2^+)^* + e\ (+e)$$
$$CO_2 + h\nu(e) \rightarrow (CO^+)^* + O + e\ (+e)$$
$$CO_2 + h\nu(e) \rightarrow CO^* + O\ (+e)$$
and, $$CO + h\nu(e) \rightarrow CO^*\ (+e)$$

The same processes occur with photoelectrons instead of solar photons but detailed analysis have shown that photoionization and photodissociation are dominant. The CO $a\,^3\Pi$ and $A\,^1\Pi$ states are also party excited by dissociative recombination of CO_2^+ and fluorescent scattering contributes partly to the $CO_2^+(A\,^2\Pi)$ and $B\,^2\Sigma$ excitation.
The OI 2972 A and the CI 1561 A and 1657 A lines are most likely produced by dissociative excitation of CO_2 as well,with a contribution by O_2^+ recombination for $O(^1S)$.
The Lyα radiation is optically thick and may be used to determine the amount of atomic hydrogen escaping from the exosphere. The ultimate source of H is photodissociation of H_2O in the lower atmosphere but the path from the lower atmosphere to the exosphere is likely indirect. It involves formation of molecular hydrogen, vertical transport and dissociation by ionospheric reaction. It is not known whether the escape flux of H depends on the water vapor mixing ratio and thus exhibits seasonal variations.
The 1304-A tripet is mainly excited by resonance scattering of $O(^3P)$ atoms in solar radiation at high altitude with a possible contribution of photoelectron impact on O and CO_2 at low altitude. The $O(^5S^\circ)$ state is populated by electron impact on O and CO_2. Since the excitation processes of most of these emissions have been established on firm grounds from the comparison of the Mars airglow spectrum and CO_2 laboratory spectra, the altitude distribution may also be used to determine the upper atmosphere scale height and density.
Table I lists the limb intensities of the main UV features observed with MARINER 6 and 7 (M6-7), Mariner 9 (M9) and the Soviet MARS 5 (M5) orbiter. The table gives total molecular system emission rates unless otherwise specified. The intensities predicted from the Fox and Dalgarno (1979) model are also given for the N_2 $C\,^3\Pi - B\,^3\Pi$ (Second Positive) and $A\,^3\Sigma - X\,^1\Sigma$ (Vegard-Kaplan) strongest bands. Although they were not observed in the MARINER spectra, these weaker features might be observable with sufficient spectral resolution and observing time. Their absolute intensities and variability would provide a way of remotely sensing molecular nitrogen. Other N_2 and N_2^+ systems are excited by photoelectron impact on molecular nitrogen, but their detection appears more difficult than the 2 Positive and Vegard-Kaplan bands. The [NI] $^4S-^2D$ emission rate at 5200 A given in table 1 is based on the $N(^2D)$ profile calculated by Fox and Dalgarno (1980). The $O_2(^1\Delta)$ (o,o) band at 1.27μm has been observed using ground-based telescopes. The intensity shows considerable variations with latitude and season. This behaviour is expected since the $O_2(^1\Delta)$ state is populated by ozone photodissociation. It provides therefore a powerful and sensitive method to determine the O_3 distribution in the lower atmosphere of Mars.

2.2. Nitric oxide fluorescence

The nitric oxide density has been measured by the VIKING 1 entry mass spectrometer (Nier and McElroy, 1977) above 115 km. The largest density observed during the descent was $6.8 \times 10^6\ cm^{-3}$ at 118 km. This value is in agreement with model calculations by Yung et al. (1977) and McElroy et al. (1977) which show a decrease below 120 km, followed by an increase below about 50 km. The NO density at the ground depends on the efficiency of its interaction with surface materials. The shape of the nitric oxide distribution depends also critically on the eddy diffusion in the lower atmosphere for which essentially no data exist so far. Von Zahn and Hunten (1982) have reviewed the various eddy coefficients used in photochemical models so far. They all tend to be two orders of magnitude larger than their terrestrial counterpart at equivalent density levels but the assumed profiles show large differences. This also accounts for the large discrepancies in the NO mixing ratio at low latitudes calculated by Yung et al. (1977) and Krasnopolsky and Parshev (1979).
The NOγ bands are partly blended with the CO($a\,^3\Pi - X\,^1\Sigma$) Cameron bands which makes the observation of the γ bands difficult. In order to investigate this problem, a synthetic spectrum of the two systems is shown in figure 2 at 0.5 A resolution. The spectrum shows the (1,0) Cameron band, the (1,0) NOγ band and the sum of the two emissions (Conway, 1982). The CO spectrum is calculated following the procedure described by Conway (1981)which provides a good fit to the MARINER 9 limb spectra. The intensity is normalized to a total system limb emission rate of 300 kR. The NOγ spectrum is calculated for resonance scattering in solar ultraviolet using a g-factor of 3.7×10^6 ph/s and a (1,0) band intensity of 2kR at 128 km, in agreement with the VIKING nitric oxide profile. Figure 3 shows a synthetic spectrum of the 1900-2500 A region at 6 Å resolution. The two spectra indicate that observation of the martian thermospheric NO is somewhat difficult for NO densities measured by VIKING; it requires a sufficient resolution and strongly depends on a good evalution of the spectral distribution of the CO hot rotational tail. Model calculations predict NO ground densities in excess of $10^8\ cm^{-3}$ and a corresponding 2150 A band intensity of 20 kR. However, the increasing contribution of the Rayleigh and Mie scattering would rapidly dominate the airglow signal at low altitudes.

2.3. The night airglow

The visible spectrometer on board the Soviet MARS 5 orbiter did not detect any nightglow emission (Krasnopolsky and Krysko, 1976). The sensitivity of the instrument puts therefore are upper limit on the emission rate of the various potential visible emissions as listed in table I. The limb intensi-

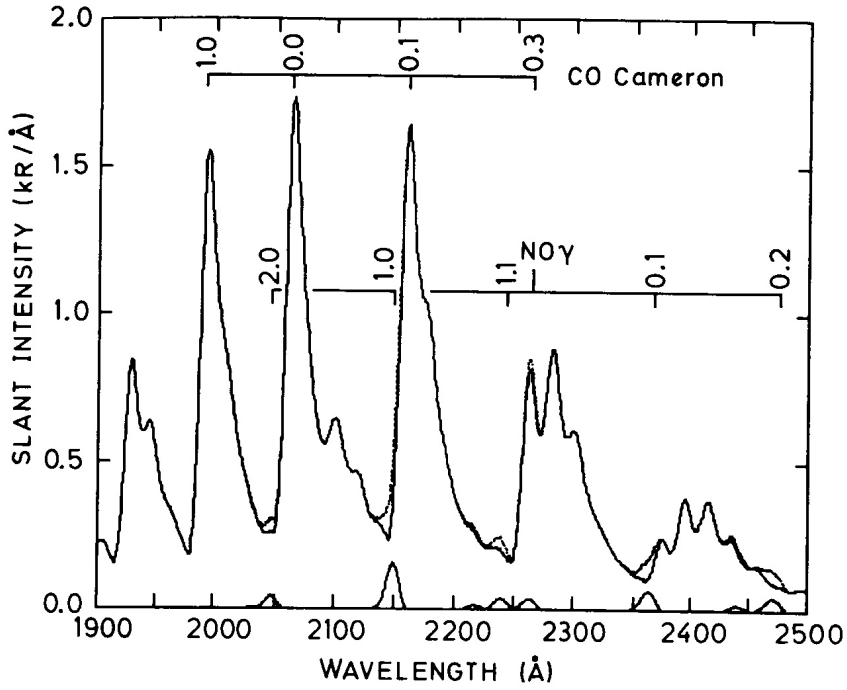

figure 3. : synthetic spectrum of the CO Cameron and NOγ systems for a 6 Å resolution. The sum of the two contributions is shown by a dotted line.

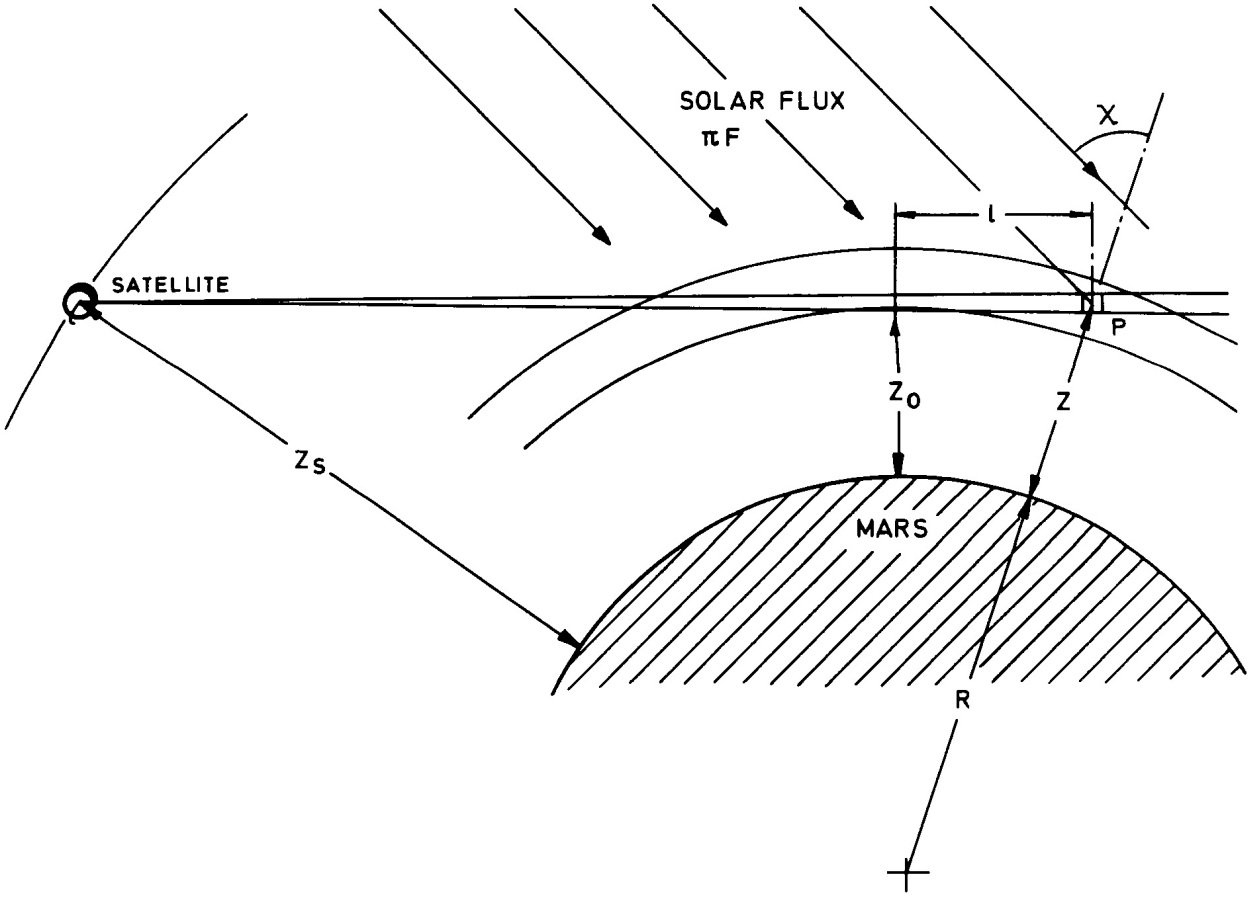

figure 4. : geometry of ultraviolet limb radiance measurements of ozone with a Mars orbiter.

Table 1.

MARS AIRGLOW EMISSION RATES

Emission	λ*(A)	Limb intensity (kR)	Reference
Day airglow			
Lyα	1216	7	M9
OI	1304	0.6	M6-7
[OI]	1356	0.5	M9
CI	1657	1.7	M6-7
NOγ(1,0)	2150	<6	M9
		2	Viking
CO 4 Positive	58	9	M6-7
CO Cameron	2185	300	M9
CO_2^+ doublet	2890	60	M9
CO_2^+ A-X	3130	140	M9
[OI]	2972	20	M9
[NI]	5200	1	estimate
[OI]	5577	400	Branching ratio
O_2 I.R.Atm.	12700	10^3-10^6	Kong-McElroy(1977)
		$2x10^3$ (disc)	Traub et al.(1979)
N_2 (2P) (0,0)	3370	0.7	Fox-Dalgarno(1979)
N_2 (V-K)(1,9)	3199	0.6	Fox-Dalgarno(1979)
Night airglow			
NOδ-γ	1980	0.001	estimate
O_2 HI	2500-3500	0.001	Krasnopolsky(1981)
O_2 HII	5000-8000	<0.03	M5
		0.04	Krasnopolsky(1981)
[OI]	5577	10^{-6}	estimate
		<0.001	M5

* The wavelength refers to the most easily observable band for molecular systems.

ties of the O_2 of the O_2 Herzberg II and II bands have been estimated by Krasnopolsky (1981), based on a comparison between atmospheric density and composition on Venus, the Earth and Mars. The predicted intensity for the OIλ5577A line is very low, due to the low atomic oxygen and high total density prevailing at 35km, compared to the conditions existing in the Earth's atmosphere at the altitude of the green line nightglow.
The nitric oxide δ and γ band recombination airglow due to radiative recombination :

$$N(^4S) + O(^3P) \rightleftarrows NO(C\,^2\Pi,\ v=o) \rightarrow NO + h\nu$$

has been observed and mapped on the night side of Venus (Stewart et al., 1980; Gérard et al., 1981). The oxygen and nitrogen atoms are carried from the day to the night side by the circulation generated by differential heating. It is also observed on Earth where its intensity declines after dusk due to the rapid recombination of nitrogen atoms. We estimate the emission rate of the total NOδ and γ systems on Mars at about 1 R at dusk, based on current odd nitrogen and oxygen martian models but unsufficient knowledge of eddy diffusion and surface chemistry makes the calculation of the diurnal variation difficult.

3. OZONE AND SCATTERED SUNLIGHT

Ozone measurements in the martian lower atmosphere have been summarized by Von Zahn and Hunten (1982) and Simon (1982). In summary, total column ozone measurements have been made with the MARINER 9 UVS, giving column densities between 60μm-atm in the winter polar region to less than 3μm-atm, the detectability threshold, at the equator. An analysis similar to the backscattered ultraviolet technique showed that the O_3 effective scale height varies between 0.2 and 0.8 $\bar{H}$, where $\bar{H}$ is the CO_2 scale height. Two ozone profiles were also derived by Krasnopolsky et al. (1977) using differential ozone absorption at 2600 and 2800 A from the MARS 5 spacecraft. The O_3 profiles peak at 2.5×10^9 and $1 \times 10^{10}\,cm^{-3}$ near 35km but such high values are difficult to accept on the basis of current odd oxygen models. In this section, we examine the use of ultraviolet limb radiance observations to determine the ozone vertical distribution on Mars. We then show that at least in certain conditions, it is possible to use a BUV technique to map the global distribution of total ozone from a spinning spacecraft.
The geometry of limb measurements of the vertical O_3 distribution is sketched in figure 4. The signal measured by the instrument is the integral of the atmospheric scattering along the line of sight. Each volume element P at altitude Z give a contribution depending on the solar flux ΠF, the density of scattering particles n(Z) and the absorption between the sun and P and between P and the satellite. As the spacecraft spins at altitude Z_s, the minimum ray height Z_o varies from 0 to Z_s. Neglecting absorption by major constituents and dust, the total signal at wavelength λ_i is thus given by

$$4\Pi I = \int_{-1}^{\infty} \Pi F(\lambda)\ \sigma_{\lambda_i}\ n(Z) P(\Psi)\ \exp(-\tau_{\lambda_i})\ dl,$$

where : l_s is the distance between the orbiter and the tangent point,
σ_{λ_i} the Rayleigh + Mie scattering cross section,
$P(\Psi)$ the phase function,
and τ_{λ_i}, the total ozone optical tickness :

$$\lambda_i = \sigma^{\circ}_{\lambda_i} \int_o^P [O_3]\,dl + \sigma^{\circ}_{\lambda_i} \int_Z^{\infty} Ch(R/H,\chi)[O_3]\ dZ,$$

with $\sigma^{\circ}_{\lambda_i}$: O_3 absorption cross section,

$Ch(R/H,\chi)$: Chapman function for scale height H and solar zenith angle χ.

By measuring the radiance as a function of Z_o, it is possible to retrieve the vertical O_3 distribution over a range of altitudes (Thomas et al., 1980). This range is defined by values of the optical thickness τ_{λ_i} between about unity and a few percent. Thus, by changing the wavelength of observation λ_i or better by observing simultaneously at several λ_i, it is possible to probe different

Table 2.

OZONE OPTICAL DEPTH FOR LIMB OBSERVATIONS							
Z_o (km)	τ_{O_3}						I_o (kR)
	$[O_3]_o = 10^9$ cm^{-3}		$[O_3]_o = 10^{10}$ cm^{-3}		$[O_3]_o = 510^{11}$ cm^{-3}		
	2550A	2900A	2550A	2900A	2550A	2900A	2800A
0	0.23	2.8(-2)	2.3	0.28	116	14	2500
10	5.5(-2)	6.8(-3)	0.55	6.8(-2)	28	3.3	920
20	1.3(-2)	-	0.13	1.6(-2)	6.6	0.8	334
40	-	-	-	-	0.38	4.7(-2)	46
60	-	-	-	-	2.2(-2)	-	6

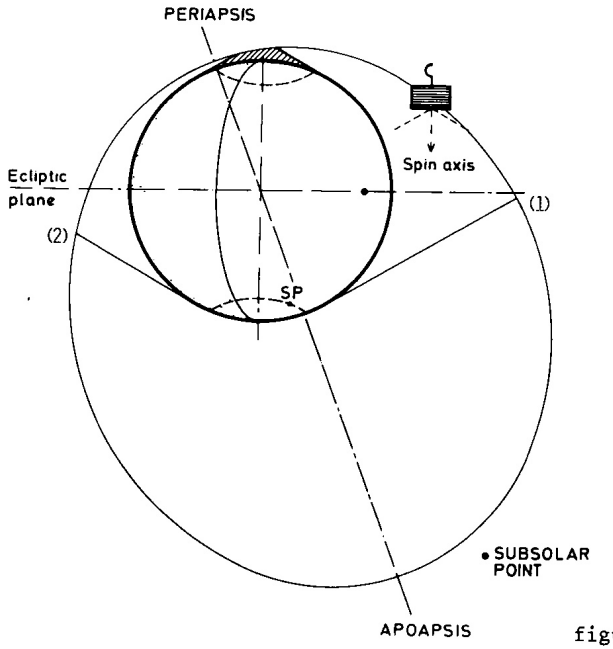

figure 5. : orbit configuration for spin-scan imaging in the case of an orbiter with spin axis perpendicular to the ecliptic plane.

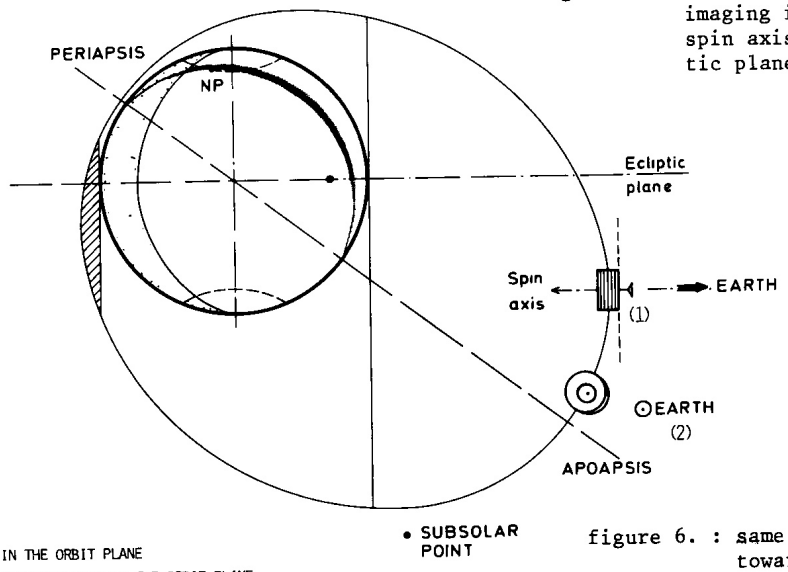

figure 6. : same as fig. 5 with spin axis oriented toward the Earth.

(1) EARTH IN THE ORBIT PLANE
(2) EARTH PERPENDICULAR TO THE ORBIT PLANE

levels of the atmosphere. Table II lists the O_3 optical thickness τ_{O_3} at 2 wavelengths as a function of the minimum ray height Z_o. The values are given at 2550 A where the O_3 aborption cross section section peak at 1.1×10^{-17} cm^2 and at 2900A where σ° is lower by a factor 8.2. The adopted ozone profile has a scale height of 5 km and O_3 surface densities of 1×10^9, 1×10^{10} and 5×10^{11} cm^{-3} are used, which cover the range of expected values from wet (equatorial) to dry (winter polar) conditions. The last column gives an estimate of the expected intensity at 2800 A. The table indicates that measurements using this technique appears feasible from the ground to 60 km in the polar regions and up to 20 km at low latitudes. A complementary technique may be used with the O_2 ($^1\Delta$) 1.27μm emission produced by ozone photolysis

$$O_3 + h\nu \rightarrow O_2 (^1\Delta_g) + O$$

It has been successfully applied to martian ozone from the ground (Traub et al., 1979) and is currently used by the Solar-Mesosphere-Explorer mission to measure mesospheric ozone (Thomas et al., 1980).

Based on available measurements and models, the vertical ozone column density varies from 1.6×10^{17} cm^{-2} to 5×10^{14} cm^{-2}. Consequently, the O_3 optical thicknesswhich is given by $2\ N_{O_3}\ \sigma^\circ$ ranges from 3.6 to 0.01 at 2550 A. Consequently, it is possible to derive the vertical daytime ozone column by measuring the backscattered ultraviolet solar radiation. Images of the sunlit martian disc may be obtained by combining the spacecraft motion and its spin. If the scattered light field is observed at several wavelengths, a two-dimensional map of the ozone field may be obtain from each orbit. This technique has been used successfully with the Dynamics Explorer imager to obtain the global ozone distribution in the terrestrial atmosphere (Keating et al., 1982) The vertical backscattered intensity for a nadir observation near 2500 A is on the order of 100 kR/Å and for pure Rayleigh scattering and the single scattering approximation is valid.

4. SPIN-SCAN IMAGING

The combination of the motion of the spacecraft along its orbit with a rapid spin makes it possible to obtain low-or medium-resolution monochromatic images of the martian disc in one or several wavelengths. This method has proven very powerful to study the morphology of airglow emissions, minor constituent distribution or localized particle induced emissions. Figure 5 shows the configuration,the imaging configuration for a 4.8 hours martian orbit with a low altitude periapsis. In this figure, the orbit is projected on a plane perpendicular to the ecliptic and containing periapsis. In the case, the spacecraft spin axis is perpendicular to the ecliptic plane and the UVS is offset 60° from the spin axis. The small circles at high latitudes represent the loci of the geographic poles during the martian year. The situation represented in fig. 5 is for winter in the Northern hemisphere when periapsis is at high Northern latitudes. The instrument's optical axis first acquires the planet from position (1) at 60° S. As the spacecraft moves toward periapsis, the line of sight scans the disc at each spin. The shaded area is the part of the orbit where the optical axis always intercepts the solid disc. At position (2), The instrument loses the planet until the next orbit. During the period between positions (1) and (2), images of the disc may be obtained with a spatial resolution depending on the instrument field of view and integration time and the distance from the planet. In the vicinity of periapsis, vertical profiles of emissions may be obtained at each spin. The period when the instrument is not in view of the planet may be used to receive telecommands and/or send stored measurements to the ground. Figure 6 illustrates the configuration for a spacecraft with the spin axis pointing to the Earth. Two particular cases are represented : the Earth in the orbit plane or perpendicular to this plane. In this configuration, the instrument is perpendicular to the satellite spin axis. In the first geometry, the entire disc may be imaged with a better resolution at the poles than at low latitudes. In the second case, the spacecraft is in the "cartwheel" mode and the spatial coverage is dratically limited. In general, an intermediate situation accurs and the spatial coverage varies during the mission between 0 and 100%.

5. DISCUSSION

We have so far briefly reviewed some of the potential measurements with a Mars spinning orbiter such as the Kepler mission. It is clear that two distinct types of measurements may be made :

- imaging of airglow and reflected sunlight at large distances from the planet.
- limb profiles and occultation measurements near periapsis.

Table III summarizes the main scientific objectives of an ultraviolet spectrometer on a spinning geophysical Mars orbiter,divided along these two observation modes. In order to achieve these objectives, the instrument must meet the following constrains :

- have a spectral scanning capability and fixed wavelength imaging mode.
- be able to observe low level airglow as well as planetary bright disc.
- be efficiently baffled against instrumentally scattered light.
- have a field of view and photon counting rate providing reasonable altitude resolution near periapsis.
- have preprogrammed observation sequences as well as the possibility of in flight interaction via telecommands.
- remain compatible with telemetry, power and weight limits of a low cost Mars mission.

6. ACKNOWLEDGEMENTS

The author is grateful to R. Conway for providing him with synthetic spectra.
He is supported by the Belgian Foundation for Scientific Research (FNRS). This research is carried out under FRFC grant Nr. 2.4507.82.

Table 3.

UVS SCIENTIFIC OBJECTIVES

Periapsis observations (z < 200km)	Apoapsis observations (z < 7000km)
I. DAYSIDE	I. DAYSIDE
- spectral mode	- bidimensional distribution of constituents : H(Lyα) : day/night, solar control, escape rate OI (1304A) : patchiness O_3 : global ozone field dust.
- vertical distribution of constituents CO_2 CO O H O_3 dust	- haze and cloud mapping
- non thermal components	- exospheric temperature (Lyα)
- alkalis and metallic ions	- surface imaging albedo topography (pressure mapping) polar caps.
- temperature profile	
II. NIGHTSIDE	II. NIGHTSIDE
- spectral mode	- nightglow mapping
- vertical distribution of nightglow layer.	- particle-induced emissions.
III. TWILIGHT	
- occultation : vertical distribution of CO_2 and O_3.	

7. REFERENCES

Barth C.A., Stewart A.I., Hord C.W. and Lane A.L., Mariner 9 ultraviolet spectrometer experiment : Mars airglow spectroscopy and variation in Lyman alpha, *Icarus, 17*, 1972.

Barth C.A., Hord C.W., Pearce J.B., Kelly K.K., Anderson G.P. and Stewart A.I., Mariner 6 and 7 ultraviolet spectrometer experiment : Upper atmosphere data, *J. Geophys. Res., 76*, 2213, 1971.

Barth C.A. et al., Mariner 9 ultraviolet spectrometer experiment : seasonal variation of ozone on Mars, *Science, 179*, 795, 1973.

Conway R.R., private communication, 1982.

Conway R.R., spectroscopy of the Cameron bands in the Mars airglow, *J.Geophys. Res., 86*,4467, 1981.

Fox J.L. and Dalgarno A., Ionization, luminosity and heating of the upper atmosphere of Mars, *J. Geophys. Res., 84*,7315, 1979.

Fox J.L. and Dalgarno A., The production of nitrogen atoms on Mars and their escape, *Planet. Space Sci., 28*, 41, 1980.

Gérard, J.C., Stewart A.I. and Bougher S.W., The altitude distribution of the Venus ultraviolet nightglow and implications on vertical transport, *geophys. Res. Lett., 8*, 633, 1981.

Keating G.M., Frank L., Craven J., Shapiro, M., Young D. and Bhartia P., Global pictures of the ozone field from high altitudes form DE-I, paper presented at the 24th Plenary meeting of COSPAR, Ottawa, 1982.

Kong T.Y. and McElroy M.B., photochemistry of the martian atmosphere, *Icarus, 32*, 168, 1977.

Krasnopolsky V.A., Excitation of oxygen emissions in the night airglow of the terrestrial planets, *Planet. Space Sci., 29*, 925, 1981.

Krasnopolsky V.A. and Krysko A.A., on the night airglow of the Martian atmosphere, *Space Res., 16*, 1005, 1976.

Krasnopolsky V.A., Krysko A.A. and Rogachev, Ultraviolet photometry of Mars on the satellite Mars 5, *Cosmic Research, 15*, 214, 1977.

Krasnopolsky V.A. and Parskev V.A., Ozone and Photochemistry of the martian lower atmosphere, *Planet. Space Sci., 27*, 113, 1979.

McElroy M.B., Kong T.Y. and Yung Y.L., Photochemistry and evolution and evolution of Mars' atmosphere a Viking perspective, *J. Geophys. Res., 82*, 4379, 1977.

Nier A.O. and McElroy, composition and structure of Mars'upper atmosphere : Results from the neutral mass spectrometers on Viking 1 and 2, *J. Geophys. Res., 82*, 4341, 1977.

Simon P.C. and Brasseur G., Ultraviolet absorption measurements in the atmosphere of Mars, *this volume*, 1982.

Stewart A.I., Mariner 6 and 7 ultraviolet spectrometer experiment : implications of CO_2^+, CO, and O airglow, *J. Geophys. Res., 77*, 54, 1972.

Stewart A.I., Barth C.A., Hord C.W. and Lane A.L., Mariner 9 ultraviolet spectrometer experiment : structure of Mars' upper atmosphere, *Icarus, 17*, 469, 1972.

Stewart A.I., Gérard J.C., Rusch D.W. and Bougher S.W., Morphology of the Venus ultraviolet night airglow, *J. Geophys. Res., 85*,7861, 1980.

Thomas G.E. et al., Scientific objectives of the Solar Mesosphere Explorer Mission, *Pageoph., 118*, 519, 1980.

Von Zahn V. and Hunten D.M., Aeronomy of Mars' lower atmosphere : status and prospects, *this volume*, 1982.

Yung Y.L., Strobel D.F., Kong T.Y. and McElroy M.B., Photochemistry of nitrogen in the martian atmosphere, *Icarus, 30*, 26, 1977.